

BootOOD: Self-Supervised Out-of-Distribution Detection via Synthetic Sample Exposure under Neural Collapse

Yuanchao Wang¹ Tian Qin¹ Eduardo Valle² Bruno Abrahao^{1,3}

¹NYU Shanghai Center for Data Science

²Intercom

³Leonard N. Stern School of Business, New York University

yw6570@nyu.edu tq2067@nyu.edu valle.do.eduardo@gmail.com abrahao@nyu.edu

Abstract

*Out-of-distribution (OOD) detection is critical for deploying image classifiers in safety-sensitive environments, yet existing detectors often struggle when OOD samples are semantically similar to the in-distribution (ID) classes. We present **BootOOD**, a fully self-supervised OOD detection framework that bootstraps exclusively from ID data and is explicitly designed to handle semantically challenging OOD samples. BootOOD synthesizes pseudo-OOD features through simple transformations of ID representations and leverages Neural Collapse (NC), where ID features cluster tightly around class means with consistent feature norms. Unlike prior approaches that aim to constrain OOD features into subspaces orthogonal to the collapsed ID means, BootOOD introduces a lightweight auxiliary head that performs radius-based classification on feature norms. This design decouples OOD detection from the primary classifier and imposes a relaxed requirement: OOD samples are learned to have smaller feature norms than ID features, which is easier to satisfy when ID and OOD are semantically close. Experiments on CIFAR-10, CIFAR-100, and ImageNet-200 show that BootOOD outperforms prior post-hoc methods, surpasses training-based methods without outlier exposure, and is competitive with state-of-the-art outlier-exposure approaches while maintaining or improving ID accuracy.*

1. Introduction

Deep neural networks achieve impressive accuracy on large-scale image classification benchmarks, yet their predictions can be brittle when inputs deviate from the training distribution. In safety-sensitive applications such as autonomous driving, medical diagnosis, and open-world recognition, this vulnerability can lead to high-confidence errors that undermine reliability. Out-of-distribution (OOD)

detection addresses this issue by equipping a classifier with the ability to detect inputs that differ from in-distribution (ID) training data and abstain or defer decisions when necessary [11, 13, 17]. Despite intensive progress, reliably detecting OOD samples remains challenging, especially when OOD data are semantically similar to ID classes.

Early work on OOD detection focused on post-hoc scoring rules applied to a frozen classifier. The simplest baseline uses the maximum softmax probability (MSP) as an OOD score [13], and subsequent methods refine this idea through calibration [11], feature-space distances [33], energy-based scores [26], gradient statistics [22], activation rectification [39], nearest neighbors [40], sparsification [38], or representation manipulation [8, 36, 43, 51]. These post-hoc methods are attractive because they can be deployed on off-the-shelf classifiers without modifying training. However, large-scale evaluations have shown that they often saturate under realistic and fine-grained distribution shifts [3, 18, 48, 53], particularly when OOD samples share visual semantics with ID classes rather than being trivially far from the training distribution.

To overcome these limitations, recent work has explored training-based OOD detectors that modify the learning objective. Some approaches adjust the classification loss to enforce calibrated confidence or explicit reject options [7, 24, 45], while others introduce auxiliary heads or embedding constraints [20, 28, 29, 41]. A dominant line of work uses outlier exposure (OE) [14], where external datasets such as synthetic noise, texture datasets, or large-scale image collections are treated as OOD and included during training. OE and its variants with virtual or synthesized outliers [9, 37, 44, 52] can significantly improve robustness, but they inherit two important limitations. First, external OOD datasets often do not comprehensively reflect the OOD samples encountered at test time, creating an OOD-distribution mismatch that limits generalization. Second, encouraging the classifier to carve out decision regions

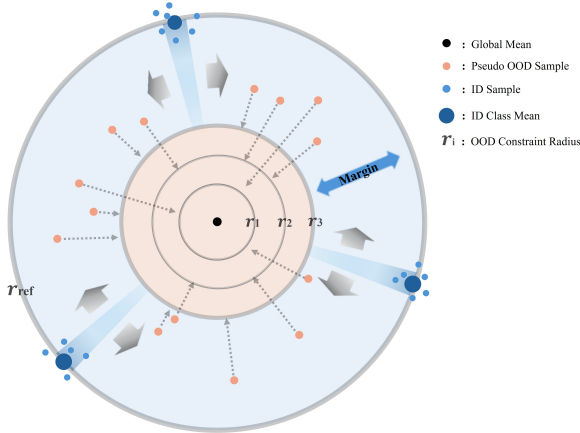


Figure 1. **Overview of the BootOOD geometry.** ID class features collapse around their class means with consistent norms under Neural Collapse. BootOOD synthesizes pseudo-OOD features in between these means and trains an auxiliary radius-based head to classify them as having smaller feature norms. The global mean defines the center, ID samples occupy a reference radius r_{ref} , and a sequence of inner radii r_1, r_2, r_3 specifies relaxed OOD constraint regions. By separating ID and OOD purely in feature-norm space, BootOOD avoids enforcing strict angular (orthogonality) constraints and relieves the main classifier from modeling OOD structure.

that separate ID classes from a wide variety of outliers can be detrimental to in-distribution accuracy and may still fail when encountering near-OOD samples that closely resemble ID classes [3, 18, 47].

Semantically similar OOD detection is especially challenging on benchmarks where ID classes occupy a dense semantic manifold. Examples include fine-grained or hierarchical label spaces such as CIFAR-100 [23], ImageNet-200 and related ImageNet-based splits [3, 34], or semantically coherent near-OOD benchmarks such as SCOOD [47]. In these settings, OOD images often come from visually related categories, for example unseen bird species or vehicles, rather than from clearly different domains such as textures [5] or scenes [54]. OpenOOD and its extensions [48, 53] highlight that many existing methods perform well on far-OOD settings yet struggle when ID and OOD classes share similar semantics. Designing detectors that explicitly target these semantically challenging regimes without sacrificing ID performance remains an open problem.

In this work, we revisit training-based OOD detection through the lens of Neural Collapse (NC) [31]. NC describes an empirical phenomenon that emerges in the terminal phase of training large classifiers, where penultimate-layer features of each class cluster tightly around their class mean, class means form an approximately equiangular tight frame, and the classifier weights align with these means. An

often underexploited aspect of NC is that the norms of ID class means and features become highly consistent across classes. Recent methods have tried to exploit NC structure by enforcing geometric constraints on OOD data during training, for example pushing them into subspaces that are orthogonal to the collapsed ID class means or enforcing large angular separation [1, 12, 25, 32, 46]. While effective in some regimes, these orthogonality-style constraints can be overly strict when ID and OOD classes are semantically similar, since realistic near-OOD samples may lie in between ID class directions rather than in strictly orthogonal subspaces.

We introduce **BootOOD**, a fully self-supervised OOD detection framework that is designed specifically for semantically similar OOD scenarios. The key idea is to relieve the main classifier from the burden of accommodating OOD data during training and to move OOD modeling into a lightweight auxiliary head that operates solely on feature norms. BootOOD bootstraps synthetic pseudo-OOD features by interpolating and perturbing ID representations that lie between collapsed class means, then trains an auxiliary radius-based classifier to regard these pseudo-OOD features as having shorter norms than ID features. This norm-based separation is a relaxed requirement compared to enforcing geometric orthogonality between ID and OOD, and it leverages the consistent norms induced by NC to define a simple radial decision rule.

Figure 1 illustrates the BootOOD geometry. ID class means form an approximate equiangular configuration around a global mean in the feature space, and ID samples concentrate near a reference radius that reflects the collapsed feature norm. BootOOD defines a sequence of inner radii that specify constraint regions for pseudo-OOD features. Synthetic OOD samples are generated between class means and trained to occupy these smaller radii, creating a margin in feature norm between ID and OOD while leaving the angular structure of the classifier largely untouched. Because the auxiliary head is decoupled from the primary classifier, BootOOD preserves ID accuracy and adds negligible computational overhead at inference.

We evaluate BootOOD on CIFAR-10, CIFAR-100, and ImageNet-200 under standard and semantically challenging OOD benchmarks [3, 23, 47, 48, 53]. BootOOD consistently improves OOD detection performance in near-OOD regimes while maintaining or improving ID accuracy. In particular, it outperforms prior post-hoc methods, surpasses training-based methods that do not rely on outlier exposure, and is competitive with state-of-the-art OE-based approaches, without requiring any real OOD data.

Our main contributions are as follows:

- We propose **BootOOD**, a self-supervised, outlier-free OOD detection framework that decouples OOD modeling from the primary classifier through a lightweight aux-

iliary head operating on feature norms, offering a more stable alternative to prior post-hoc and training-based approaches in semantically similar OOD regimes.

- We leverage Neural Collapse to formulate a relaxed norm-based separation between ID and OOD features, and introduce a bootstrapping strategy that synthesizes pseudo-OOD features lying between collapsed class means, avoiding the strict geometric (e.g., orthogonality) constraints required by recent NC-based methods.
- We demonstrate that BootOOD delivers strong OOD performance on CIFAR-10, CIFAR-100, and ImageNet-200, outperforming prior post-hoc and outlier-free training-based methods and remaining competitive with outlier exposure approaches, while maintaining ID accuracy.

2. Related Work

2.1. Post-hoc OOD Detection

Post-hoc OOD detection methods operate on a fixed classifier and design scoring rules to distinguish ID and OOD samples at test time. The MSP baseline [13] uses the maximum softmax probability as an uncertainty score, and calibration techniques [11] further adjust confidence without changing the underlying classifier. Distance-based approaches compute scores from penultimate features, for example Mahalanobis distances to class-conditional Gaussians [33] or Gram-matrix statistics [35]. Energy-based methods [26] interpret OOD detection in terms of the log-sum-exp of logits and can be combined with various training objectives.

Beyond logits and distances, other post-hoc approaches exploit gradients [22], activation rectification [39], virtual-logit matching [43], deep nearest neighbors [40], sparsification [38], rank-one feature removal [36], or simple activation shaping [8]. Hopfield-style energy models [51] and confidence branches [7] provide additional alternatives. These methods typically require no extra training and are widely adopted due to their simplicity and compatibility with pretrained models.

However, comprehensive evaluations on large-scale and semantically rich benchmarks [3, 18, 48, 53] show that post-hoc methods often plateau when OOD samples are semantically similar to ID classes. In particular, near-OOD benchmarks such as SCOOD [47] and ImageNet-based settings that use fine-grained or hierarchically related OOD classes [3, 34] reveal that many post-hoc scores are sensitive to the underlying representation and struggle to separate overlapping semantic manifolds.

2.2. Training-based OOD Detection Without Outlier Exposure

Training-based OOD detectors modify the learning objective in order to produce representations or logits that are in-

trinsically more amenable to OOD detection. Confidence-calibrated classifiers [7, 24] encourage low confidence on hard or adversarial examples and provide explicit reject options. LogitNorm [45] normalizes logits to mitigate overconfidence and improves the calibration of decision boundaries. Methods based on hyperspherical embeddings [29] or nonparametric synthesis [28, 41] design geometric or sampling constraints that separate ID and implicitly defined OOD directions without relying on external outlier datasets. Self-supervised learning has also been used to improve robustness and uncertainty estimation [15]. Unlike prior work that leverages self-supervision primarily to enhance in-distribution feature learning, our BootOOD framework uses self-supervision to explicitly model OOD data. Instead of enriching ID representations, we generate and refine OOD-aware supervisory signals that guide the network to better characterize, separate, and detect out-of-distribution samples.

These approaches avoid the practical difficulties of collecting and maintaining external OOD corpora, and they are often more stable when ID labels are fixed. Yet when semantically similar OOD samples are considered, the training objective may still place a heavy burden on the primary classifier. Enforcing complex geometry on top of the classification loss can distort decision regions and lead to an unfavorable trade-off between ID accuracy and OOD performance [2, 10]. BootOOD falls into this category of outlier-free training-based methods, but it explicitly decouples OOD modeling from the main classifier through an auxiliary norm-based head.

2.3. Training-based Methods with Outlier Exposure

Outlier exposure [14] trains the classifier with an additional loss on external OOD data, encouraging uniform or low-confidence predictions on outlier samples. OE has inspired a variety of extensions that either refine the choice of outlier datasets or synthesize virtual outliers. VOS [9] learns virtual outlier synthesis in feature space. MixOE [52] and related methods [37, 44] construct mixture or repaired OOD samples that better cover the semantic space. Other works integrate OE with large-scale robustness techniques such as AugMix [16] or specialize to particular evaluation settings [18, 21].

While OE-style methods can achieve strong performance, their reliance on external outlier collections raises questions about coverage and domain mismatch [17, 18]. In near-OOD regimes, even carefully chosen OE datasets may not align with the fine-grained semantics of the ID task, and the need to accommodate a wide variety of outliers within the primary classifier can degrade ID accuracy. In contrast, BootOOD does not require any real OOD data and instead bootstraps pseudo-OOD features directly from ID representations.

2.4. Neural Collapse and Feature Norm for OOD Detection

Neural Collapse has emerged as a unifying perspective on the geometry of deep classifiers at convergence [31]. Beyond explaining training dynamics, NC has motivated OOD and open-set recognition methods that exploit the structure of collapsed features and classifier weights. NECO [1], feature separation approaches [46], and NC-inspired detectors [12, 25] enforce geometric constraints on synthetic or real OOD samples, often by encouraging them to lie in subspaces orthogonal to ID class means or by manipulating feature norms. Park et al. [32] further analyze the role of feature norms for OOD detection and show that norm statistics carry useful information about distributional shifts. These methods highlight that neural-collapse-induced structure can serve as a powerful inductive bias for OOD detection, yet many existing approaches still couple OOD constraints directly to the classifier and rely on strong angular-separation assumptions between ID and OOD samples [1, 46].

BootOOD differs in two key aspects. First, it leverages the consistent norms of NC to formulate a relaxed, purely radial separation between ID and OOD, rather than enforcing strict orthogonality. Second, it delegates OOD modeling to an auxiliary radius-based head that consumes both ID and bootstrapped pseudo-OOD features, which reduces interference with the classifier responsible for ID accuracy. As we show in our experiments, this design is particularly effective for semantically similar OOD benchmarks on CIFAR-10, CIFAR-100, and ImageNet-200.

3. Methodology

3.1. Problem Setup

We consider supervised image classification with inputs $x \in \mathbb{R}^d$ and categorical labels $y \in \{1, \dots, C\}$. A backbone network $f_\theta : \mathbb{R}^d \rightarrow \mathbb{R}^m$ extracts penultimate-layer features

$$h(x) = f_\theta(x),$$

and a linear classifier $W = [w_1, \dots, w_C]^\top \in \mathbb{R}^{C \times m}$ produces logits

$$z(x) = Wh(x).$$

Training uses only in-distribution (ID) data; no real OOD samples are used.

To simplify notation, we denote

$$\text{norm}(u) = \frac{u}{\|u\|_2},$$

and we use $\hat{u} = \text{norm}(u)$ for L2-normalized vectors.

3.2. Pseudo-OOD Feature Generation

Given an ID minibatch with features $\{h_i\}_{i=1}^B$, we generate pseudo-OOD features directly in the feature space. Two distinct features (h_i, h_j) are randomly paired, and we sample $\lambda \sim \text{Beta}(\alpha, \alpha)$ to form a mixed representation

$$h_{\text{ood}} = \lambda h_i + (1 - \lambda) h_j, \quad i \neq j. \quad (1)$$

Thus, all pseudo-OOD samples used during training arise from *feature-level mixup of ID features*, without relying on any external OOD data.

We denote the normalized pseudo-OOD feature as

$$\tilde{h} = \hat{h}_{\text{ood}}.$$

3.3. Tracking the ID Feature Geometry

BootOOD leverages the Neural Collapse (NC) geometry that naturally emerges during late-phase cross-entropy training. To model this geometry, we maintain two exponential moving averages (EMAs):

ID feature mean

$$\mu \leftarrow \beta_\mu \mu + (1 - \beta_\mu) \bar{h}_{\text{ID}}, \quad (2)$$

ID feature radius

$$r_{\text{ref}} \leftarrow \beta_r r_{\text{ref}} + (1 - \beta_r) \|h - \mu\|_2. \quad (3)$$

The scalar r_{ref} captures the collapsed ID radius, while μ tracks the global ID center; β_* are hyperparameters for the EMA.

3.4. Radius-Based Organization of Pseudo-OOD Samples

We discretize the interval $[0, r_{\text{ref}}]$ into K inner-shell target radii

$$0 < \rho_1 < \rho_2 < \dots < \rho_K < r_{\text{ref}},$$

e.g., via uniform or cosine spacing. A lightweight radius head $g_\phi : \mathbb{R}^m \rightarrow \mathbb{R}^K$ maps \tilde{h} to a distribution over shells.

Given a sampled shell index s , we optimize:

Radius classification

$$\mathcal{L}_{\text{cls}} = \text{CE}(g_\phi(\tilde{h}), s). \quad (4)$$

Radius regression

$$\mathcal{L}_{\text{reg}} = \left(\|\tilde{h} - \mu\|_2 - \rho_s \right)^2. \quad (5)$$

This encourages pseudo-OOD features to populate well-defined inner shells of decreasing radius, separating them from the ID outer shell near r_{ref} .

3.5. Directional Separation

To further decouple pseudo-OOD features from ID classifier directions, we impose a soft angular-separation penalty:

$$\mathcal{L}_{\text{sep}} = \mathbb{E}_c \left[\left| \langle \hat{h}, \hat{w}_c \rangle \right| \right], \quad (6)$$

computed with the classifier weights W detached. This is motivated by recent findings that enforcing angular disentanglement improves OOD detection [46].

3.6. Total Objective

ID samples are optimized with standard cross-entropy:

$$\mathcal{L}_{\text{CE}} = \text{CE}(z(x), y).$$

We define the pseudo-OOD loss as

$$\mathcal{L}_{\text{OOD}} = \lambda_{\text{cls}} \mathcal{L}_{\text{cls}} + \lambda_{\text{reg}} \mathcal{L}_{\text{reg}}.$$

The full training objective is

$$\mathcal{L} = \mathcal{L}_{\text{CE}} + \lambda_{\text{ood}}(t) \mathcal{L}_{\text{OOD}} + \lambda_{\text{sep}}(t) \mathcal{L}_{\text{sep}}, \quad (7)$$

where $\lambda_{\text{ood}}(t)$ and $\lambda_{\text{sep}}(t)$ follow simple linear warm-up schedules. The radius head parameters ϕ are introduced as a separate optimizer group.

3.7. Training Algorithm

Algorithm 1 summarizes the full BootOOD training procedure. Each iteration updates the ID classifier using standard cross-entropy, while simultaneously organizing mixed pseudo-OOD features into inner-radius shells and enforcing angular separation.

Why Mixup-Generated Pseudo-OOD Targets Near-OOD. Near-OOD samples are known to lie in the *low-density, between-class* region of the ID feature space and often behave as **interpolations** between ID semantic manifolds [32, 40]. This region corresponds to the complement of high-density class neighborhoods within the convex hull:

$$\text{Conv}(\{z_c\}) \setminus \bigcup_c \mathcal{N}(z_c).$$

Mixup as surrogate near-OOD. Feature-level mixup,

$$z_{\text{mix}} = \lambda z_i + (1 - \lambda) z_j, \quad \lambda \sim \text{Beta}(\alpha, \alpha),$$

guarantees that $z_{\text{mix}} \in \text{Conv}(\{z_c\})$, and therefore places pseudo-OOD exactly in this *between-class* low-density region.

NC geometry. Under Neural Collapse, ID class means form a Simplex ETF [31]; convex combinations lie on its *faces*, which are the natural decision boundaries. Thus mixup features fall near ETF faces—the same geometric zone where near-OOD typically appears.

Algorithm 1: BootOOD Training Procedure

Input: Training set \mathcal{D}_{ID} , backbone f_θ , classifier W , radius head g_ϕ

Init: EMA mean μ , EMA radius r_{ref} , schedules $\lambda_{\text{ood}}(t)$ and $\lambda_{\text{sep}}(t)$

1 for each training iteration do

/* --- ID forward pass --- */

2 Sample minibatch $(x_i, y_i)_{i=1}^B \sim \mathcal{D}_{\text{ID}}$;

3 Compute ID features $h_i = f_\theta(x_i)$ and logits $z_i = W h_i$;

4 Update EMA center μ using Eq. (2);

5 Update EMA radius r_{ref} using Eq. (3);

6 Compute ID loss $\mathcal{L}_{\text{CE}} = \text{CE}(z_i, y_i)$;

/* Pseudo-OOD feature generation */

7 **for** $k = 1$ **to** M **do**

Randomly pick $i \neq j$ from $\{1, \dots, B\}$;

Sample $\lambda \sim \text{Beta}(\alpha, \alpha)$;

$h_{\text{ood}}^{(k)} = \lambda h_i + (1 - \lambda) h_j$;

$\tilde{h}^{(k)} = \text{norm}(h_{\text{ood}}^{(k)})$;

/* Radius-based OOD modeling */

12 Sample shell index $s \sim \{1, \dots, K\}$;

13 Compute radius-classification loss \mathcal{L}_{cls} via Eq. (4);

14 Compute radius-regression loss \mathcal{L}_{reg} via Eq. (5);

/* Directional separation */

15 Compute angular-separation loss \mathcal{L}_{sep} via Eq. (6);

/* Total loss and update */

16 $\mathcal{L} = \mathcal{L}_{\text{CE}} + \lambda_{\text{ood}}(t) (\lambda_{\text{cls}} \mathcal{L}_{\text{cls}} + \lambda_{\text{reg}} \mathcal{L}_{\text{reg}}) + \lambda_{\text{sep}}(t) \mathcal{L}_{\text{sep}}$;

17 Update θ , ϕ , and W using $\nabla \mathcal{L}$;

Table 1. Compatibility of Our Method w/ Various PostProcessors

Method	CIFAR-10		CIFAR-100		ImageNet-200	
	FPR@95	AUROC	FPR@95	AUROC	FPR@95	AUROC
EBO[26]	64.19(±0.67)	87.65(±0.53)	53.17(±0.57)	81.98(±0.53)	63.16(±0.45)	80.79(±0.38)
Entropy[27]	62.71(±0.33)	88.32(±0.43)	51.03 (±0.36)	83.09 (±0.23)	58.65(±0.34)	82.95(±0.32)
ReAct[39]	76.73(±0.74)	87.01(±0.81)	54.65(±0.55)	81.95(±0.43)	65.50(±1.58)	81.18(±1.50)
Norm[32, 50]	31.34 (±0.27)	92.40 (±0.28)	98.83(±1.08)	43.09(±1.23)	79.11(±0.83)	74.75(±0.80)
MSP[13]	62.32(±0.41)	89.17(±0.43)	53.28(±0.77)	82.31(±0.51)	53.16 (±0.22)	84.16 (±0.20)

Inference and OOD scoring. At test time we discard the radius head and use only the backbone and classifier. Given a test image, we obtain its logits and penultimate feature and compute five post-hoc OOD scores. We compare these five scores across datasets and OOD sets in Table 1. Thresholds for binary ID/OOD decisions are chosen on a held-out ID validation split (e.g., a fixed percentile on ID scores) or following the OpenOOD evaluation protocol.

4. Experiments

4.1. Datasets, Protocols, and Metrics

Protocol. We follow the standard **OpenOOD v1.5** protocol [53]: models are trained on *ID-only* data and evaluated on held-out ID/OOD sets. All experiments use ResNet-18 with input resolution 32×32 for CIFAR-10/100 and 224×224 for ImageNet-200. Results are reported as mean \pm std over **3 seeds**, and initialization uses the corresponding OpenOOD pretrained checkpoints.

OOD sets and near/far rationale. For CIFAR-10 as ID, the near-OOD pool contains CIFAR-100 and Tiny-ImageNet (TIN) with overlapping classes removed [23]; the far-OOD pool contains MNIST [6], SVHN [30], Textures [5], and Places365 [54]. For CIFAR-100 as ID, the near-OOD pool is CIFAR-10 and TIN, and the far-OOD pool matches the CIFAR-10 setting. For ImageNet-200 as ID, following OpenOOD, the near-OOD pool uses SSB-Hard and NINCO [3]; the far-OOD pool consists of iNaturalist [19], Textures, and OpenImage-O [43].

Data usage. BootOOD uses ID-only training and ID-only validation. Real OOD samples are never used during training; pseudo-OOD arises solely from our feature-level generator. When a baseline requires OOD validation (e.g., temperature scaling), we follow OpenOOD and draw a small disjoint OOD validation split from the designated OOD pool.

Evaluation. We validate using multiple post-processors—entropy[27], norm[32, 50], ReAct[39], EBO[26], and MSP[13]. Because different datasets favor different scoring rules, we select the post-processor that achieves the best performance on the *ID-only validation split*, and use that fixed scorer for final testing. The backbone is unchanged at test time; only the scoring rule differs.

Metrics. We report AUROC, FPR95, $AUPR_{IN}$, $AUPR_{OUT}$, and ID-ACC. Thresholds for FPR95/TNR95 follow OpenOOD and are determined on a held-out validation split. OOD test labels are never used for model selection.

Neural-Collapse warm-up. To ensure Phase 1 reaches the Neural Collapse regime before Phase 2, we require training ID-only data beyond zero training error : NC typically appears around ~ 70 epochs on CIFAR-10, ~ 80 on CIFAR-100, and ~ 100 on ImageNet-200.

4.2. Baselines

We follow the OpenOOD v1.5 taxonomy and compare it with representative methods with respect to performance and recency of publication from three categories: post-hoc inference, outlier-free training, and outlier-exposed training. The complete list of methods and their respective settings is presented in the Appendix.

4.3. Main Results

We compare **BootOOD** against representative methods from the three standard OOD categories in OpenOOD: *post-hoc* methods, *training-time* methods without real OOD, and *training-time* methods with real OOD (four baselines per category). Following the OpenOOD protocol and its leaderboard focus, we report results on the *near-OOD* setting only, which is widely regarded as the most challenging regime. For CIFAR-10/100 and ImageNet-200, all numbers in Table 2 are averaged over **3** random seeds.

CIFAR-10. *BootOOD* achieves higher AUROC and lower FPR95 than all post-hoc methods and all training-time methods without outlier data. The largest gains appear on the *near-OOD* split (CIFAR-100/TIN), where closeness to ID makes separation difficult.

CIFAR-100. On this more fine-grained ID dataset, *BootOOD* surpasses *all* OpenOOD v1.5 post-hoc methods and *all* training-time methods, *including* those that leverage auxiliary outlier data (OE/MCD/UDG/MixOE). The advantage is especially pronounced on near-OOD (CIFAR-10/TIN), indicating that our radius-regularized representation improves class-conditional compactness and inter-class separation. Compared with the additional NECO and Feature Separation baselines, *BootOOD* also leads consistently while preserving ID-ACC.

ImageNet-200. Using the same ResNet-18 backbone with 224^2 inputs, *BootOOD* outperforms every OpenOOD v1.5 post-hoc method and all training-time methods *without* outlier data. Improvements are most visible on near-OOD (SSB-Hard/NINCO) where many categories are fine-grained and visually similar to ID. We also find that *BootOOD* is competitive with methods that rely on additional outliers even though it does not use them.

Discussion of trends and failure modes. Across datasets, the largest relative improvements occur on *near-OOD*, corroborating recent findings that near-OOD is intrinsically more challenging than far-OOD [3, 42]. Our radius-based regularization most benefits categories with heavy inter-class confusion, where tightening ID manifolds reduces spurious high confidence on semantically similar

Table 2. Near-OOD: CIFAR-10, CIFAR-100 and ImageNet-200.

Category	Method	AUROC	FPR @95%	AUPR IN	AUPR OUT	ID-ACC
CIFAR-10 (ID Acc: 95.22±0.30)						
Posthoc	SHE[51]	80.84(±1.30)	84.48(±1.10)	75.53(±2.30)	81.93(±1.39)	95.22 (±0.30)
	RMDS[33]	89.53(±0.35)	42.19(±0.31)	89.79(±0.26)	87.48(±0.34)	95.22 (±0.30)
	KNN[40]	90.70(±0.10)	34.54(±0.22)	91.73(±0.21)	88.71(±0.36)	95.22 (±0.30)
	NECO[1]	91.52(±2.63)	37.32(±0.61)	91.86(±1.42)	90.23 (±1.01)	95.22 (±0.30)
	BootOOD (Ours)	92.40 (±0.28)	31.34 (±0.27)	93.75 (±0.36)	89.94(±0.35)	95.08 (±0.43)
	Train (w/o)	NPOS[41]	83.31(±0.31)	45.02(±0.42)	86.82(±0.36)	76.49(±0.27)
PFS[46]		89.10(±1.25)	37.38(±0.83)	89.67(±0.96)	81.01(±1.04)	86.06(±0.54)
ConfBranch[7]		89.84(±0.24)	31.97(±0.13)	91.72(±0.29)	85.84(±0.54)	94.24(±0.11)
CIDER[29]		90.26(±0.20)	32.94(±0.34)	91.88(±0.18)	87.72(±0.27)	N/A
BootOOD (Ours)		92.40 (±0.28)	31.34 (±0.27)	93.75 (±0.36)	89.94 (±0.35)	95.08 (±0.43)
Train (with)		MixOE[52]	88.57(±0.88)	56.07(±0.74)	86.43(±0.86)	87.61(±0.69)
	MCD[49]	89.21(±0.14)	25.65(±0.21)	88.80(±0.18)	91.21(±1.15)	93.67(±0.04)
	UDG[47]	89.77(±0.24)	36.18(±0.26)	90.65(±0.19)	87.05(±0.17)	93.77(±0.87)
	OE[14]	94.14 (±0.21)	19.65 (±0.33)	94.57 (±0.28)	93.88 (±0.19)	94.24(±0.24)
	BootOOD (Ours)	92.40 (±0.28)	31.34 (±0.27)	93.75 (±0.36)	89.94(±0.35)	95.08 (±0.43)
	CIFAR-100 (ID Acc: 77.19±0.13)					
Posthoc	NECO[1]	47.91(±0.50)	95.57(±0.20)	50.94(±0.35)	45.70(±0.32)	71.35(±0.13)
	SHE[51]	78.24(±0.28)	59.30(±0.18)	82.15(±0.26)	72.04(±0.30)	77.09(±0.13)
	TempScale[11]	81.46(±0.27)	54.78(±0.07)	84.03(±0.20)	74.87(±0.22)	77.43(±0.13)
	MLS[18]	81.56(±0.23)	55.48(±0.07)	83.88(±0.18)	74.93(±0.22)	77.19(±0.13)
	BootOOD (Ours)	83.09 (±0.23)	51.03 (±0.36)	84.93 (±0.24)	77.65 (±0.28)	78.89 (±0.12)
	Train (w/o)	PFS[46]	72.19(±0.40)	61.59(±0.30)	77.04(±0.35)	62.12(±0.40)
NPOS[41]		74.41(±0.37)	67.11(±0.26)	78.21(±0.24)	66.72(±0.28)	N/A
MOS[21]		80.74(±0.18)	55.06(±0.20)	83.39(±0.18)	73.87(±0.20)	76.62(±0.20)
VOS[9]		81.02(±0.29)	54.99(±0.18)	83.81(±0.22)	74.19(±0.24)	77.09(±0.10)
BootOOD (Ours)		83.09 (±0.23)	51.03 (±0.36)	84.93 (±0.24)	77.65 (±0.28)	78.89 (±0.12)
Train (with)		UDG[47]	77.63(±0.20)	60.39(±0.22)	81.06(±0.18)	71.22(±0.24)
	MCD[49]	79.72(±0.25)	57.81(±0.30)	82.05(±0.22)	73.11(±0.24)	74.98(±0.38)
	MixOE[52]	79.88(±1.77)	60.38(±0.95)	67.40(±0.55)	85.27 (±0.70)	71.93(±0.64)
	OE[14]	80.88(±0.20)	55.04(±0.18)	83.84(±0.16)	74.89(±0.20)	75.30(±0.42)
	BootOOD (Ours)	83.09 (±0.23)	51.03 (±0.36)	84.93 (±0.24)	77.65 (±0.28)	78.89 (±0.12)
	ImageNet-200 (ID Acc: 86.37±0.09)					
Posthoc	NECO[1]	55.89(±0.92)	86.98(±0.58)	45.81(±0.35)	63.92(±0.42)	86.37(±0.09)
	SHE[51]	80.18(±0.53)	66.80(±0.32)	64.25(±0.26)	84.20(±0.24)	86.37(±0.09)
	TempScale[11]	83.24(±0.33)	57.29(±0.32)	69.04(±0.27)	88.38 (±0.25)	86.37(±0.09)
	MSP[13]	83.34(±0.38)	54.82(±0.30)	68.96 (±0.24)	85.95(±0.25)	86.37(±0.09)
	BootOOD (Ours)	84.16 (±0.28)	53.01 (±0.28)	68.17(±0.30)	86.78(±0.65)	86.60 (±0.15)
	Train (w/o)	NPOS[41]	74.41(±0.37)	67.11(±0.26)	78.21 (±0.24)	66.72(±0.28)
CIDER[29]		80.72(±1.38)	61.40(±0.48)	66.20(±0.38)	80.70(±0.42)	N/A
ARPL[4]		82.10(±0.18)	63.80(±0.34)	67.70(±0.26)	84.05(±0.28)	84.10(±0.34)
LogitNorm[45]		82.42(±0.22)	57.06(±0.34)	67.73(±0.26)	86.22(±0.30)	86.48(±0.18)
BootOOD (Ours)		84.16 (±0.28)	53.01 (±0.28)	68.17(±0.30)	86.78 (±0.65)	86.60 (±0.15)
Train (with)		UDG[47]	71.63(±1.52)	66.42(±0.95)	76.19(±0.72)	66.73(±0.80)
	MixOE[52]	80.05(±0.07)	59.61(±0.21)	81.68 (±0.18)	72.93(±0.20)	85.01(±0.10)
	MCD[49]	81.42(±0.38)	61.03(±0.27)	79.85(±0.22)	70.58(±0.25)	85.12(±0.26)
	OE[14]	85.02 (±0.24)	53.16(±0.22)	70.51(±0.22)	86.85 (±0.26)	85.90(±0.18)
	BootOOD (Ours)	84.16 (±0.28)	53.01 (±0.28)	68.17(±0.30)	86.78(±0.65)	86.60 (±0.15)

CIDER[29] and NPOS[41] train the CNN backbone without the final linear classifier, and the official implementations do not provide code for evaluating ID accuracy.

OODs. Typical failure cases arise when near-OOD samples lie extremely close to decision boundaries (e.g., fine-grained bird species vs. ImageNet-200 classes); in those cases the score distributions can partially overlap, and improvements rely on careful tuning of the ramp schedule and margin. On far-OOD, improvements are consistent but smaller because separability is already easier.

4.4. Feature geometry analysis on CIFAR-100.

To inspect what *BootOOD* learns, we plot the distributions of (i) feature *radius* $\|\mathbf{z}\|_2$ and (ii) the maximum cosine to class weights $\max_c \cos(\mathbf{z}, \mathbf{w}_c)$ over ID test images and pseudo-OOD samples gathered at inference. As shown in

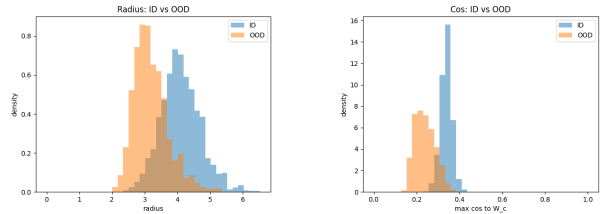


Figure 2. CIFAR-100 feature diagnostics: (left) radius $\|\mathbf{z}\|_2$; (right) max cosine to class weights $\max_c \cos(\mathbf{z}, \mathbf{w}_c)$. ID (blue) vs. pseudo-OOD (orange).

Fig. 2 (left), ID features concentrate at larger radii while pseudo-OOD concentrate at smaller radii, with only a narrow overlap near the boundary; this matches the design of our radius self-supervision that encourages compact, larger-norm ID manifolds and discourages large norms for OOD-like points. In Fig. 2 (right), ID samples exhibit consistently higher maximal cosine to some class prototype than pseudo-OOD, indicating that ID features align more strongly with class directions whereas pseudo-OOD remain less aligned. Together, the two diagnostics corroborate the mechanism observed in the ablations: the *radius* terms provide the primary separability (clear norm gap), and the *feature separation* term further reduces alignment of pseudo-OOD with any class, which helps especially on near-OOD. We found the same qualitative pattern across seeds, and the operating thresholds selected on validation are therefore stable.

On the seemingly small cosine for ID. Note that the ID histogram in Fig. 2(right) peaks around 0.3 – 0.4, which may look modest despite strong AUROC. This is expected because the class logit decomposes as $\ell_c = \mathbf{w}_c^\top \mathbf{z} = \|\mathbf{w}_c\| \|\mathbf{z}\| \cos \theta_c$. Our method primarily increases separability through the *radius* term: ID features have larger $\|\mathbf{z}\|$ while pseudo-OOD have smaller $\|\mathbf{z}\|$ (Fig. 2, left), so the dot product (and related energy scores) remains well separated even when $\cos \theta$ is moderate. Moreover, in high dimensions the maximum cosine over 100 classes need not be large to be discriminative, and we do not enforce a cosine (unit-norm) classifier; hence the model leverages *norm* \times *moderate alignment* rather than extreme alignment. This explains why AUROC is high while the ID cosine values are not; the norm gap is the main driver, with cosine providing complementary margins, especially near class boundaries.

4.5. Ablations and Design Choices

We conduct ablations on **CIFAR-100** (ResNet-18), averaging results over all near-/far-OOD test sets. We independently remove: (1) the *Phase-1* warm-up, (2) the *radius self-supervision* losses (rad-cls & rad-reg), (3) the *feature-separation* loss, and (4) vary the number of *radius bins* K used by the training-time radius head. Table 3 and Table 4

Table 3. Ablation study on CIFAR-100 using ResNet-18. Results show relative changes (%) with respect to the full BootOOD model. Removing any component degrades OOD detection (lower AUROC, higher FPR@95%).

Setting	Δ AUROC (%) \uparrow	Δ FPR@95% \downarrow	Δ ID-ACC (%) \uparrow
BootOOD (full)	—	—	—
w/o Phase-1 warm-up	-2.6	+9.7	-1.1
w/o radius self-supervision	-4.2	+5.3	-1.3
w/o feature separation	-0.7	+1.0	-0.8

report relative changes against the full model.

Phase-1 warm-up. Removing the Phase-1 warm-up leads to a clear drop in AUROC (-2.6%) and a large increase in FPR@95% ($+9.7\%$). This shows that letting the classifier first learn stable ID prototypes before turning on OOD regularization is important for both ID accuracy and OOD detection.

Radius self-supervision. Ablating the radius self-supervision ($\mathcal{L}_{\text{rad-cl}} + \lambda_{\text{mse}}\mathcal{L}_{\text{rad-reg}}$) hurts performance the most (-4.2% AUROC). Once these losses are removed, the model behaves close to plain CE training, and the feature norms no longer provide a strong ID vs. OOD separation signal.

Feature separation. Dropping the feature separation term yields a smaller but consistent degradation (-0.7% AUROC, higher FPR@95%). Thus, separation is not the main driver but still gives a useful extra margin, especially for near-OOD close to class boundaries.

Effect of radius bins K . We also vary the number of radius bins K in the training-only radius head that supervises pseudo-OOD radii. As shown in Table 4, $K = 1$ (pure regression without meaningful radius classes) performs worst, while increasing K initially improves near-OOD AUROC and FPR@95 by providing a richer discretization of the inner-shell targets. Performance peaks at $K = 4$ and then slightly degrades for $K = 6$, suggesting that too many bins introduce unnecessary quantization noise without clear benefits. We therefore adopt $K = 4$ as our default.

Summary. All components matter: Phase-1 warm-up provides stability, radius self-supervision is the main driver of OOD separability, feature separation adds complementary gains, and a moderate number of radius bins ($K=4$) yields the best near-OOD performance.

Table 4. Near-OOD ablation on the number of radius bins K in the training-time radius head (CIFAR-100).

K (radius bins)	AUROC	FPR@95%
$K = 1$	77.67(± 0.72)	62.35(± 0.61)
$K = 3$	80.46(± 0.39)	56.47(± 0.41)
$K = 4$	83.09 (± 0.23)	51.03 (± 0.36)
$K = 6$	81.88(± 0.16)	53.58(± 0.26)

5. Conclusion and Future Work

Conclusion. We presented **BootOOD**, a *training-time*, ID-only OOD detector that exploits late-phase Neural Collapse geometry to shape a simple feature-norm score. On CIFAR-10/100 and ImageNet-200 within OpenOOD—where *near-OOD* is both the most challenging regime and the key leaderboard criterion—BootOOD significantly improves near-OOD AUROC and FPR95 while preserving ID top-1 accuracy. A lightweight radius head is used only during training: we synthesize pseudo-OOD features via mixup, supervise them with inner-shell radius targets, and add a directional separation penalty; the inference path remains unchanged.

Future Work.

- **Richer pseudo-OOD generators.** Beyond feature-space mixup, we have implemented column-element shuffle and block-shuffle generators; they tend to help far-OOD more than near-OOD and are therefore omitted from the main tables. A natural extension is to combine these generators in a unified objective or curriculum to jointly optimize near- and far-OOD performance.
- **Broader backbones and theory.** Applying BootOOD to larger or multimodal backbones and open-set or long-tailed settings, and further analyzing how Neural Collapse geometry aligns with radius-based scores and ID-only calibration, are promising directions.

References

- [1] Mouin Ben Ammar, Nacim Belkhir, Sebastian Popescu, Antoine Manzanera, and Gianni Franchi. Neco: Neural collapse based Out-of-Distribution detection. In *ICLR*, 2024. 2, 4, 7
- [2] Julian Bitterwolf, Alexander Meinke, Maximilian Augustin, and Matthias Hein. Breaking down out-of-distribution detection: Many methods based on ood training data estimate a combination of the same core quantities. In *International Conference on Machine Learning*, 2022. 3
- [3] Julian Bitterwolf, Maximilian Müller, and Matthias Hein. In or out? fixing imagenet Out-of-Distribution detection evaluation. In *Proceedings of the 40th International Conference on Machine Learning (ICML)*, pages 2471–2506, 2023. 1, 2, 3, 6

- [4] Guanyao Chen, Peixi Peng, Xiangqian Wang, and Yonghong Tian. Adversarial reciprocal points learning for open set recognition. *IEEE TPAMI*, 44(11):8065–8081, 2022. 7
- [5] Mircea Cimpoi, Subhransu Maji, Iasonas Kokkinos, Sammy Mohamed, and Andrea Vedaldi. Describing textures in the wild. In *CVPR*, pages 3606–3613, 2014. 2, 6
- [6] Li Deng. The MNIST database of handwritten digit images for machine learning research [best of the web]. *IEEE Signal Processing Magazine*, 29(6):141–142, 2012. 6
- [7] Terrance DeVries and Graham W. Taylor. Learning confidence for Out-of-Distribution detection in neural networks. *arXiv preprint arXiv:1802.04865*, 2018. 1, 3, 7
- [8] Andrija Djurisic, Nebojsa Bozanic, Arjun Ashok, and Rosanne Liu. Extremely simple activation shaping for Out-of-Distribution detection. In *ICLR, 2023*. 1, 3
- [9] Xuefeng Du, Zhaoning Wang, Mu Cai, and Yixuan Li. Vos: Learning what you don’t know by virtual outlier synthesis. In *ICLR, 2022*. 1, 3, 7
- [10] Zhen Fang, Yixuan Li, Jie Lu, Jiahua Dong, Bo Han, and Feng Liu. Is out-of-distribution detection learnable? In *NeurIPS, 2022*. 3
- [11] Chuan Guo, Geoff Pleiss, Yu Sun, and Kilian Q. Weinberger. On calibration of modern neural networks. In *Proceedings of the 34th International Conference on Machine Learning (ICML)*, pages 1321–1330, 2017. 1, 3, 7
- [12] Jarrod Haas, William Yolland, and Bernhard T. Rabus. Linking neural collapse and l2 normalization with improved out-of-distribution detection in deep neural networks. *Transactions on Machine Learning Research*, 2023. 2, 4
- [13] Dan Hendrycks and Kevin Gimpel. A baseline for detecting misclassified and Out-of-Distribution examples in neural networks. In *ICLR, 2017*. 1, 3, 5, 6, 7
- [14] Dan Hendrycks, Mantas Mazeika, and Thomas G. Dietterich. Deep anomaly detection with outlier exposure. In *ICLR*, 2019. 1, 3, 7
- [15] Dan Hendrycks, Mantas Mazeika, Saurav Kadavath, and Dawn Song. Using self-supervised learning can improve model robustness and uncertainty. In *NeurIPS*, pages 15637–15648, 2019. 3
- [16] Dan Hendrycks, Norman Mu, Ekin D. Cubuk, Barret Zoph, Justin Gilmer, and Balaji Lakshminarayanan. Augmix: A simple data processing method to improve robustness and uncertainty. In *ICLR, 2020*. 3
- [17] Dan Hendrycks, Steven Basart, Norman Mu, Saurav Kadavath, Frank Wang, Evan Dorundo, Rahul Desai, Tyler Zhu, Samyak Parajuli, Mike Guo, Dawn Song, Jacob Steinhardt, and Justin Gilmer. The many faces of robustness: A critical analysis of out-of-distribution generalization. *arXiv preprint arXiv:2006.16241*, 2021. 1, 3
- [18] Dan Hendrycks, Steven Basart, Mantas Mazeika, Andy Zou, Joseph Kwon, Mohammadreza Mostajabi, Jacob Steinhardt, and Dawn Song. Scaling out-of-distribution detection for real-world settings. In *Proceedings of the 39th International Conference on Machine Learning (ICML)*, pages 8759–8773, 2022. 1, 2, 3, 7
- [19] Grant Van Horn, Oisín Mac Aodha, Yang Song, Yin Cui, Chen Sun, Alex Shepard, Hartwig Adam, Pietro Perona, and Serge Belongie. The inaturalist species classification and detection dataset. In *CVPR*, pages 8769–8778, 2018. 6
- [20] Yen-Chang Hsu, Yilin Shen, Hongxia Jin, and Zolt Kira. Generalized ODIN: Detecting Out-of-Distribution image without learning from Out-of-Distribution data. In *CVPR*, pages 10951–10960, 2020. 1
- [21] Rui Huang and Yixuan Li. Mos: Towards scaling Out-of-Distribution detection for large semantic space. In *CVPR*, pages 8710–8719, 2021. 3, 7
- [22] Rui Huang, Andrew Geng, and Yixuan Li. On the importance of gradients for detecting distributional shifts in the wild. In *NeurIPS*, pages 677–689, 2021. 1, 3
- [23] Alex Krizhevsky. Learning multiple layers of features from tiny images. Technical report, University of Toronto, 2009. 2, 6
- [24] Kimin Lee, Honglak Lee, Kibok Lee, and Jinwoo Shin. Training confidence-calibrated classifiers for detecting out-of-distribution samples. In *ICLR, 2018*. 1, 3
- [25] Litian Liu and Yao Qin. Detecting out-of-distribution through the lens of neural collapse. In *ICLR, 2024*. 2, 4
- [26] Weitang Liu, Xiaoyun Wang, John D. Owens, and Yixuan Li. Energy-based out-of-distribution detection. In *NeurIPS*, 2020. 1, 3, 5, 6
- [27] Xixi Liu, Yaroslava Lochman, and Christopher Zach. Gen: Pushing the limits of softmax-based out-of-distribution detection. In *CVPR*, pages 23946–23955, 2023. 5, 6
- [28] Yifei Ming, Ying Fan, and Yixuan Li. Poem: Out-of-distribution detection with posterior sampling. In *International Conference on Machine Learning*, 2022. 1, 3
- [29] Yifei Ming, Yiyu Sun, Ousmane Dia, and Yixuan Li. How to exploit hyperspherical embeddings for Out-of-Distribution detection? In *ICLR, 2023*. 1, 3, 7
- [30] Yuval Netzer, Tao Wang, Adam Coates, Alessandro Bisacco, Bo Wu, and Andrew Y. Ng. Reading digits in natural images with unsupervised feature learning. In *NIPS Workshop on Deep Learning and Unsupervised Feature Learning*, 2011. 6
- [31] Vardan Papyan, X. Y. Han, and David L. Donoho. Prevalence of neural collapse during the terminal phase of deep learning training. *Proceedings of the National Academy of Sciences*, 117(40):24652–24663, 2020. 2, 4, 5
- [32] Jaewoo Park, Jacky Chen Long Chai, Jaeho Yoon, and Andrew Beng Jin Teoh. Understanding the feature norm for out-of-distribution detection. In *ICCV, 2023*. 2, 4, 5, 6
- [33] Jie Ren, Stanislav Fort, Jeremiah Liu, Abhijit Guha Roy, Shreyas Padhy, and Balaji Lakshminarayanan. A simple unified framework for detecting Out-of-Distribution samples and adversarial attacks. In *NeurIPS*, pages 7167–7177, 2018. 1, 3, 7
- [34] Tal Ridnik, Emanuel Ben-Baruch, Asaf Noy, and Lihi Zelnik-Manor. Imagenet-21k pretraining for the masses. In *NeurIPS, 2021*. 2, 3
- [35] Chandramouli Shama Sastry and Sageev Oore. Detecting Out-of-Distribution examples with Gram matrices. In *Proceedings of the 37th International Conference on Machine Learning (ICML)*, pages 8491–8501, 2020. 3

- [36] Yue Song, Nicu Sebe, and Wei Wang. Rankfeat: Rank-1 feature removal for Out-of-Distribution detection. In *NeurIPS*, 2022. 1, 3
- [37] Rui Sun, Andi Zhang, Haiming Zhang, Jinke Ren, Yao Zhu, Ruimao Zhang, Shuguang Cui, and Zhen Li. Sr-ood: Out-of-distribution detection via sample repairing. *arXiv preprint arXiv:2305.18228*, 2023. 1, 3
- [38] Yiyu Sun and Yixuan Li. Dice: Leveraging sparsification for Out-of-Distribution detection. In *ECCV*, pages 691–708, 2022. 1, 3
- [39] Yiyu Sun, Chuan Guo, and Yixuan Li. React: Out-of-Distribution detection with rectified activations. In *NeurIPS*, pages 144–157, 2021. 1, 3, 5, 6
- [40] Yiyu Sun, Yifei Ming, Xiaojin Zhu, and Yixuan Li. Out-of-distribution detection with deep nearest neighbors. In *Proceedings of the 39th International Conference on Machine Learning (ICML)*, pages 20827–20840, 2022. 1, 3, 5, 7
- [41] Leitian Tao, Xuefeng Du, Xiaojin Zhu, and Yixuan Li. Non-parametric outlier synthesis. In *ICLR*, 2023. 1, 3, 7
- [42] Sagar Vaze, Kai Han, Andrea Vedaldi, and Andrew Zisserman. Open-set recognition: A good closed-set classifier is all you need? In *ICLR*, 2022. 6
- [43] Haoqi Wang, Zhizhong Li, Litong Feng, and Wayne Zhang. Vim: Out-Of-Distribution with virtual-logit matching. In *CVPR*, pages 4911–4920, 2022. 1, 3, 6
- [44] Qizhou Wang, Zhen Fang, Yonggang Zhang, Feng Liu, Yixuan Li, and Bo Han. Learning to augment distributions for out-of-distribution detection. In *NeurIPS*, 2023. 1, 3
- [45] Hongxin Wei, Renchunzi Xie, Hao Cheng, Lei Feng, Bo An, and Yixuan Li. Mitigating neural network overconfidence with logit normalization. In *Proceedings of the 39th International Conference on Machine Learning (ICML)*, pages 23631–23644, 2022. 1, 3, 7
- [46] Yingwen Wu, Ruiji Yu, Xinwen Cheng, Zhengbao He, and Xiaolin Huang. Pursuing feature separation based on neural collapse for Out-of-Distribution detection. In *ICLR*, 2025. 2, 4, 5, 7
- [47] Jingkang Yang, Haoqi Wang, Litong Feng, Xiaopeng Yan, Huabin Zheng, Wayne Zhang, and Ziwei Liu. Semantically coherent Out-of-Distribution detection. In *ICCV*, pages 8301–8309, 2021. 2, 3, 7
- [48] Jingkang Yang, Pengyun Wang, Dejian Zou, Zitang Zhou, Kunyuan Ding, Wenxuan Peng, Haoqi Wang, Guangyao Chen, Bo Li, Yiyu Sun, Xuefeng Du, Kaiyang Zhou, Wayne Zhang, Dan Hendrycks, Yixuan Li, and Ziwei Liu. Openood: Benchmarking generalized out-of-distribution detection. In *NeurIPS*, 2022. 1, 2, 3
- [49] Qing Yu and Kiyoharu Aizawa. Unsupervised Out-of-Distribution detection by maximum classifier discrepancy. In *ICCV*, pages 9518–9526, 2019. 7
- [50] Yeonguk Yu, Sungho Shin, Seongju Lee, Changhyun Jun, and Kyoobin Lee. Block selection method for using feature norm in out-of-distribution detection. In *CVPR*, 2023. 5, 6
- [51] Jinsong Zhang, Qiang Fu, Xu Chen, Lun Du, Zelin Li, Gang Wang, Xiaoguang Liu, Shi Han, and Dongmei Zhang. Out-of-distribution detection based on in-distribution data patterns memorization with modern hopfield energy. In *ICLR*, 2023. 1, 3, 7
- [52] Jingyang Zhang, Nathan Inkawhich, Randolph Linderman, Yiran Chen, and Hai Li. Mixture outlier exposure: Towards Out-of-Distribution detection in fine-grained environments. In *Proceedings of the IEEE/CVF Winter Conference on Applications of Computer Vision (WACV)*, pages 5531–5540, 2023. 1, 3, 7
- [53] Jingyang Zhang, Jingkang Yang, Pengyun Wang, Haoqi Wang, Yueqian Lin, Haoran Zhang, Yiyu Sun, Xuefeng Du, Yixuan Li, Ziwei Liu, Yiran Chen, and Hai Li. Openood v1.5: Enhanced benchmark for out-of-distribution detection. *Data-centric Mach. Learn. Res. (DMLR)*, 2024. 1, 2, 3, 6
- [54] Bolei Zhou, Agata Lapedriza, Aditya Khosla, Aude Oliva, and Antonio Torralba. Places: A 10 million image database for scene recognition. *IEEE TPAMI*, 40(6):1452–1464, 2018. 2, 6